

# Phase-locked array of quantum cascade lasers with an integrated Talbot cavity

Lei Wang,<sup>1, 2</sup> Jinchuan Zhang,<sup>2</sup> \* Zhiwei Jia,<sup>2</sup> Yue Zhao,<sup>2</sup> Chuanwei Liu,<sup>2</sup> Yinghui Liu,<sup>2</sup> Shenqiang Zhai,<sup>2</sup> Zhuo Ning,<sup>2, \*\*</sup> Xiangang Xu,<sup>1, \*\*\*</sup> and Fengqi Liu<sup>2</sup>

<sup>1</sup>*State Key Laboratory of Crystal Materials, Shandong University, Jinan 250100, People's Republic of China.*

<sup>2</sup>*Key Laboratory of Semiconductor Materials Science, Institute of Semiconductors, Chinese Academy of Sciences, P.O. Box 912, Beijing 100083, People's Republic of China.*

\*[zhangjinchuan@semi.ac.cn](mailto:zhangjinchuan@semi.ac.cn); \*\*[zhuoning@semi.ac.cn](mailto:zhuoning@semi.ac.cn); \*\*\*[xxu@sdu.edu.cn](mailto:xxu@sdu.edu.cn)

**Abstract:** We show a phase-locked array of three quantum cascade lasers with an integrated Talbot cavity at one side of the laser array. The coupling scheme is called diffraction coupling. By controlling the length of Talbot to be a quarter of Talbot distance ( $Z_t/4$ ), in-phase mode operation can be selected. The in-phase operation shows great modal stability under different injection currents, from the threshold current to the full power current. The far-field radiation pattern of the in-phase operation contains three lobes, one central maximum lobe and two side lobes. The interval between adjacent lobes is about  $10.5^\circ$ . The output power is about 1.5 times that of a single-ridge laser. Further studies should be taken to achieve better beam performance and reduce optical losses brought by the integrated Talbot cavity.

## Introduction

Since first demonstrated in 1994,<sup>1</sup> quantum cascade lasers (QCLs) have proven to be ideal laser sources in the mid-infrared spectral region, thanks to the features of compact size, room temperature operation, and high reliability.<sup>2</sup> In this spectral region, many applications such as atmospheric environmental monitoring,<sup>3</sup> breath analysis,<sup>4</sup> and infrared countermeasures<sup>5</sup> demand sources with high output power and well beam quality. Increasing the width of laser ridge is the most direct way to get high output power. However, simply widening the laser ridge will lead to high-order transverse mode operation and then results in poor beam equality. There are two directions to overcome this problem. First, some special optical designs may be taken for broad area devices to ensure fundamental transverse mode operation. Such reports include photonic crystal DFB lasers<sup>6</sup>, master-oscillator power-amplifiers<sup>7</sup>, angled cavity lasers<sup>8</sup>, and tilted facet lasers<sup>9</sup>. Second, we can integrate several narrow-ridge lasers in parallel on a single chip and phase-lock the lasers with a constant phase shift through some specific coupling schemes. This is called phase-locked array technology. Phase-locked array with in-phase operation can provide coherent light with beam divergence smaller than that of a single laser<sup>10</sup>. Recently, this technology have been intensively studied for QCLs, including evanescent-wave coupling arrays<sup>11, 12</sup>, leaky wave coupling arrays<sup>13, 14</sup>, Y-coupling arrays<sup>15</sup> and global antenna mutual coupling arrays.<sup>16</sup> However, the evanescent-wave coupling devices often tend to favor out-of-phase operation;<sup>11</sup> leaky-wave coupling devices can operate in in-phase mode but need very complex regrowth process to form anti-waveguides structure<sup>13</sup> or need additional phase sectors;<sup>14</sup> Y-coupling devices often show undesirable self-pulsation dynamics between in-phase and out-of-phases operation due to spatial hole burning effect;<sup>14</sup> global antenna mutual coupling scheme is only suitable for surface-emitting laser with a deep subwavelength confined cavity.<sup>16</sup>

Talbot effect is a well-known optical phenomenon that the intensity pattern of an array of coherent emitters reproduces itself after a specific distance of propagation.<sup>17</sup> This effect has been exploited to phase-lock lasers in the near-infrared, which is called diffraction coupling scheme phase-locked array.<sup>10</sup> In this method, a flat mirror should be placed in front of the cavity surface of the laser array to provide optical feedback. The space between the cavity surface and the flat mirror is called Talbot cavity. To

support the in-phase operation, the length of Talbot cavity should be a quarter of the Talbot distance,  $Z_t/4$ , if we define

$$Z_t = \frac{nd^2}{\lambda}, \quad (1)$$

where  $n$  is the refractive index in Talbot cavity;  $d$  is the center-to-center spacing between adjacent lasers in the array;  $\lambda$  is the wavelength. Obviously, this technology is also suitable for mid-infrared QCLs. In this article, we have realized a phase-locked array of three mid-infrared QCLs with an integrated Talbot cavity.

## Device and design

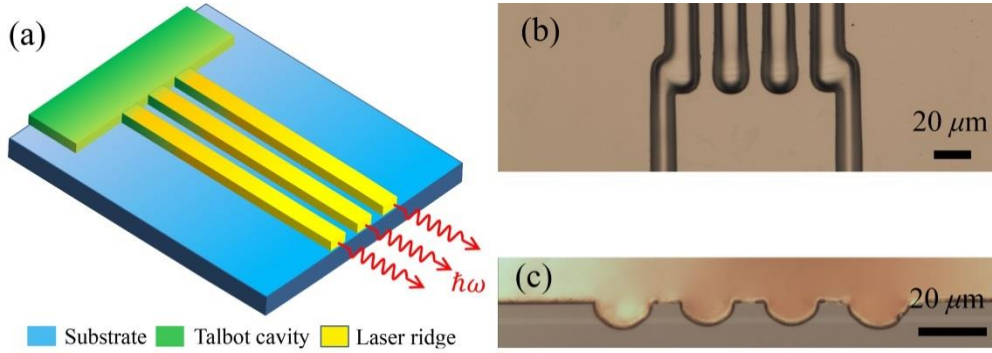


Fig. 1. (a) Sketch of the array device. (b) Microscope picture of the wafer after standard photolithographic and wet chemical etching process. (c) Microscope picture of fabricated three-laser array

Fig. 1 shows the sketch and microscope pictures of the device. The device contains an array of three lasers and an integrated Talbot cavity. The width of the laser ridge is about 12  $\mu\text{m}$  to ensure fundamental transverse mode operation. The center-to-center spacing between adjacent lasers in the array is 25  $\mu\text{m}$ , and the length of each laser ridge is 2mm. The integrated Talbot cavity is a broad and non-etched region.

The Threshold condition of the array device can be expressed by

$$r_1 r_2 \eta \cdot \exp[2 \cdot (g - \alpha_w) \cdot (L_l + L_T)] = 1, \quad (2)$$

$$g = \alpha_w + \frac{1}{2(L_l + L_T)} \ln \frac{1}{r_1 r_2} + \frac{1}{2(L_l + L_T)} \ln \frac{1}{\eta}, \quad (3)$$

where  $r_1$  and  $r_2$  are the facet reflectivities;  $\eta$  is the coupling efficiency when the light couples into the cavity of laser array after propagating a round trip in the Talbot cavity;  $g$  is the differential gain;  $\alpha_w$  is the waveguide loss;  $L_l$  is the length of laser ridge;  $L_T$  is the length of Talbot cavity. The Eq. (2) can be expressed by

$$g = \alpha_w + \alpha_m + \alpha_\eta, \quad (4)$$

where  $\alpha_m$  is the mirror loss, representing the second term in equation Eq. (2);  $\alpha_\eta$  is the coupling loss when light couples into the cavity of laser array after propagating a round trip in the Talbot cavity, representing the third term. Obviously,  $\alpha_w$  and  $\alpha_m$  have nearly no difference between in-phase and out-phase mode operation. Therefore, modal selection mainly depends on  $\alpha_\eta$  and therefore the coupling efficiency  $\eta$ .

Because there is no optical confinement in the array direction in the Talbot cavity, the light emitted from the laser array can diffract freely in this direction. Therefore, the propagating of light in the Talbot cavity can be characterized by the radiation of an array of one-dimension Gaussian sources. The  $\eta$  can be calculated by the overlap integral<sup>18</sup>

$$\eta = \frac{\left| \int E(x)E_0^*(x)dx \right|^2}{\int E(x)E^*(x)dx \int E(x)E_0^*(x)dx}. \quad (5)$$

Here, the integration area is the interface between the Talbot cavity and laser array; x-axis is along the array direction;  $E_0(x)$  is the array mode profile, which can be characterized by an array of one-dimension Gaussian sources;  $E(x)$  is the optical field after the light emitted from the laser array propagates a round trip in Talbot cavity. It can be characterized by the radiation profile of an array of one-dimension Gaussian sources at the propagation distance equal to twice  $L_T$ . Fig. 2 shows the calculated  $\eta$  as a function of  $L_T$ . The in-phase mode will have greater  $\eta$  than out-of-phase mode if  $L_T$  is between about 75  $\mu\text{m}$  and 125  $\mu\text{m}$ . In this range, the  $\eta$  of in-phased mode reaches the maximum if  $L_T$  is near  $Z_t/4$  (about 100  $\mu\text{m}$ ; here the refraction index  $n$  in Eq. (1) should be the effective index in the Talbot cavity). Therefore, in order to fabricate devices with in-phase operation, the  $L_T$  should be  $Z_t/4$ .

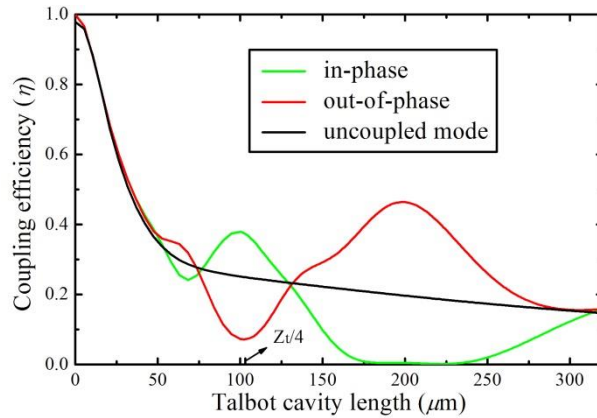


Fig. 2. Calculated coupling efficiency as a function of Talbot cavity length

## Experimental results and discussion

The fabrication and measurement of the devices are the same as discussion in Ref 19. Measured lateral far-field radiation pattern of arrays with  $L_T$  equal to  $Z_t/4$  is shown in Fig. 3a. It clearly reflects in-phase operation. The far-filed radiation pattern of array contains a central maximum lobe and two side lobes. The intensities of side lobes are nearly half the intensity of the central lobe. The interval between adjacent lobes is about 10.5°. Such a far-filed profile indicates that the beam divergence of the device is smaller than that of a single laser with 12- $\mu\text{m}$ -width ridge (horizontal beam divergence of 4.6  $\mu\text{m}$  QCLs with 12- $\mu\text{m}$ -width ridge is about 32° for fundamental transverse mode operation). The in-phase operation shows great modal stability under different injection currents, from the threshold current to the full power current. This is an advantage compared to some other coupling schemes such as evanescent-wave coupling arrays, and Y-coupling arrays.

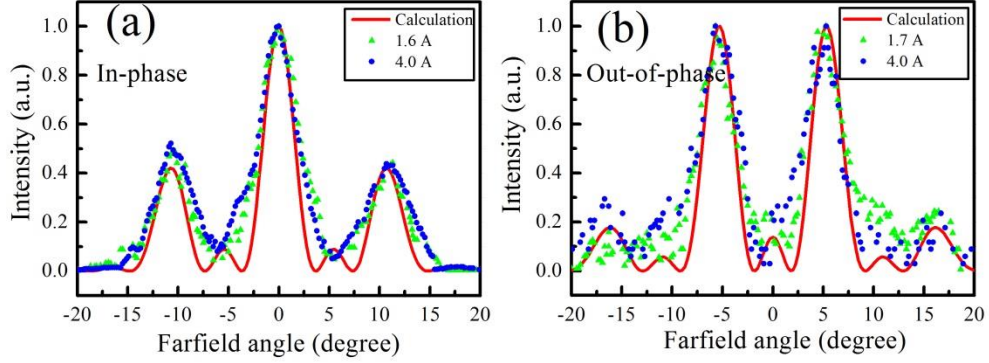


Fig. 3. Measured far-field radiation patterns of arrays with either in-phase or out-of-phase operation. Far-field profile of either in-phase or out-of phase mode is calculated through Fourier transform of the array mode profile.

The far-field radiation pattern can be interpreted by the multi-slit Fraunhofer diffraction theory<sup>20</sup>

$$F(\theta) = I(\theta)G(\theta), \quad (6)$$

where  $F(\theta)$  is the array far-field;  $I(\theta)$  is far-field of an individual laser in the array;  $G(\theta)$  is called grating function, represent the multi-slit interference effect. The interval between central maximum lobe and side lobes  $\delta\theta$  is determined by  $G(\theta)$ , interference effect, and can be calculated by

$$d \cdot \delta\theta = \lambda. \quad (7)$$

The calculated result of  $\delta\theta$  is about  $10.6^\circ$ , which is nearly same with the experimental result. Because the full width at half maximum (FWHM) of  $I(\theta)$ , beam divergence of a single-ridge laser, is about  $32^\circ$ , three interference peaks are contained in this range. This is why the measured far-field profile contains three lobes. To get single-lobe far-field profile, we can decrease the center to center spacing of adjacent lasers in the array to increase the  $\delta\theta$  or increase the width of ridge to decrease the FWHM of  $I(\theta)$ , so that only one interference peak can be contained in the range of FWHM of  $I(\theta)$ .

As a contrast, we also fabricated devices with  $L_T$  equal to  $Z_t/2$ . Measured far-field radiation pattern of such devices is shown in Fig. 3b. The measured far-field profile reflects out-of-phase operation. Two peaks locate at  $5.2^\circ$ ,  $-5.2^\circ$  respectively. What we must notice is that the two peaks have opposite phase.

Fig. 4 is the optical power-current (P-I) characterization of uncoated devices in pulse mode (pulse width  $1\mu\text{s}$  and duty cycle 1.5%). The heat sink was kept at 283 K. The device with the length of Talbot cavity of  $Z_t/4$  (in-phase) exhibits a maximum power of 375 mW, a slope efficiency of 0.15 W/A, and a threshold current density of  $1.9 \text{ kA/cm}^2$  (threshold current is  $1.55 \text{ A}$ ; current injection area is about  $8 \times 10^{-4} \text{ cm}^2$ ); the device with the length of Talbot cavity of  $Z_t/2$  (out-of-phase) exhibits a maximum power of 300 mW, a slope efficiency of 0.13 W/A, and a threshold current density of  $1.9 \text{ kA/cm}^2$  (threshold current is  $1.7 \text{ A}$ ; current injection area is about  $8.8 \times 10^{-4} \text{ cm}^2$ ). They show the nearly same threshold current densities. The latter has greater threshold current because of longer Talbot cavity. We also measured P-I curve of a normal single-ridge laser for comparison (the laser ridge is  $12\text{-}\mu\text{m-wide}$  and  $2\text{-mm-long}$ ). The single-ridge device shows a maximum power of 250 mW, a slope efficiency of 0.29 W/A and a threshold current density of  $1.6 \text{ kA/cm}^2$ . It can be found that the integrated Talbot cavity could result in slightly increase in threshold current density and obviously decrease in slope efficiency. As a result, the maximum power of the array is just about 1.5 times that of a single-ridge laser. The performance degradation is because of serious optical losses brought by the integrated Talbot cavity: (a) The Talbot image is not well matching with the origin. This results in small  $\eta$ , when the light couples into the laser array from the Talbot cavity (according to Fig. 2a, the  $\eta$  is approximately 40% for

in-phase mode, and 50% for out-of-phase mode); (b) from the Fig. 1b, the laser ridges near the Talbot cavity show taper shape. Such shape is formed because of nonuniform distribution of etching solutions in this area during the wet chemical etching process. Such Taper shape will also lead to additional cavity losses.

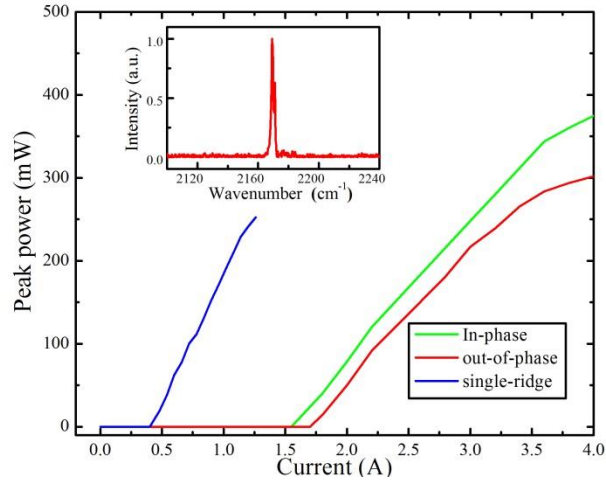


Fig. 4. Measured P-I curve lines of array devices and a single-ridge device. The insert is the measured emission spectrum.

Further studies should be taken to reduce the optical losses brought by the integrated Talbot cavity. A redesigned Talbot cavity geometry has been reported,<sup>21</sup> where all the laser elements in the arrays are tilted toward a common aim point and the  $L_T$  is  $Z_t/2$ . Such geometry can support the in-phase mode with significantly reduced loss. This geometry may be suitable for our devices.

## Conclusion

In conclusion, three QCLs have been phase-locked in an array, through integrating a Talbot cavity at one side of the laser array. In-phase mode operation can be obtained by controlling  $L_T$  equal to  $Z_t/4$ . The three-laser array with an integrated cavity shows a maximum power 1.5 times that of a single-ridge device, and a smaller beam divergence. The in-phase operation shows great modal stability under different injection currents, from the threshold current to the full power current, which is achieved through simple fabrication process. This is an advantage over other coupling schemes. Further studies should be taken to obtain better beam quality and reduce the losses brought by the integrated Talbot cavity.

## References

1. J. Faist, F. Capasso, D. L. Sivco, C. Sirtori, A. L. Hutchinson, and A. Y. Cho, “Quantum cascade laser,” *Science* **264**(**5158**), 553–556 (1994).
2. Y. Yao, A. J. Hoffman, and C. F. Gmachl, “Mid-infrared quantum cascade lasers,” *Nat. Photonics* **6**(**7**), 432–439 (2012).
3. J. Barry McManus, Mark S. Zahniser, David D. Nelson, Joanne H. Shorter, Scott Herndon, Ezra Wood, and Rick Wehr, “Application of quantum cascade lasers to high-precision atmospheric trace gas measurements” *Opt. Eng.* **49**(**11**), 111124 (2010).
4. Wörle K1, Seichter F, Wilk A, Armacost C, Day T, Godejohann M, Wachter U, Vogt J, Radermacher P, and Mizaikoff B, “Breath Analysis with Broadly Tunable Quantum Cascade Lasers,” *Anal. Chem.* **85**(**5**), 2697–2702 (2013).

5. Andrew Sijan, "Development of Military Lasers for Optical Countermeasures in the Mid-IR," Proc. SPIE. **7483**, 748304 (2009).
6. Y. Bai, S. R. Darvish, S. Slivken, P. Sung, J. Nguyen, A. Evans, W. Zhang, and M. Razeghi, "Electrically pumped photonic crystal distributed feedback quantum cascade lasers," Appl. Phys. Lett. **91**(14), 141123 (2007).
7. Patrick Rauter, Stefan Menzel, Anish K. Goyal, Christine A. Wang, Antonio Sanchez, George Turner, and Federico Capasso, "High-power arrays of quantum cascade laser master-oscillator power-amplifiers," Opt. Express **21**(4), 4518–4530 (2013).
8. Y. Bai, S. Slivken, Q. Lu, N. Bandyopadhyay, and M. Razeghi, "Angled cavity broad area quantum cascade lasers," Appl. Phys. Lett. **101**(8), 081106 (2012).
9. S. Ahn, C. Schwarzer, T. Zederbauer, D. C. MacFarland, H. Detz, A. M. Andrews, W. Schrenk, and G. Strasser, "High-power, low-lateral divergence broad area quantum cascade lasers with a tilted front facet," Appl. Phys. Lett. **104**(5), 051101 (2014).
10. Gary A. Evans and Jacob M. Hammer, *Surface Emitting Semiconductor Lasers and Arrays* (Academic, 1981), Chap. 8.
11. G. M. de Naurois, M. Carras, B. Simozrag, O. Patard, F. Alexandre, and X. Marcadet, "Coherent quantum cascade laser micro-stripe arrays," AIP Adv. **1**(3), 032165 (2011).
12. Y. H. Liu, J. C. Zhang, F. L. Yan, F. Q. Liu, N. Zhuo, L. J. Wang, J. Q. Liu, and Z. G. Wang, "Coupled ridge waveguide distributed feedback quantum cascade laser arrays," Appl. Phys. Lett. **106**(14), 142104 (2015).
13. J. D. Kirch, C. C. Chang, C. Boyle, L. J. Mawst, D. Lindberg, T. Earles, and D. Botez, "5.5 W near-diffraction-limited power from resonant leaky-wave coupled phase-locked arrays of quantum cascade lasers," Appl. Phys. Lett. **106**(6), 061113 (2015).
14. T. Y. Kao, Q. Hu, and J. L. Reno, "Phase-locked arrays of surface-emitting terahertz quantum-cascade lasers," Appl. Phys. Lett. **96**(10), 101106 (2010).
15. Arkadiy Lyakh, Richard Maulini, Alexei Tsekoun, Rowel Go, and C. Kumar N. Patel, "Continuous wave operation of buried heterostructure  $4.6\text{ }\mu\text{m}$  quantum cascade laser Y-junctions and tree arrays," Opt. Express **22**(1), 1203–1208 (2014).
16. Tsung-Yu Kao, John L. Reno, and Qing Hu, "Phase-locked laser arrays through global antenna mutual coupling," Nat. Photonics **10**(8), 541–546 (2016).
17. Jianming Wen, Yong Zhang, and Min Xiao, "The Talbot effect: recent advances in classical optics, nonlinear optics, and quantum optics," Adv. Opt. Photon. **5**(1), 83–130 (2013).
18. D. G. Hall, R. R. Rice, and J. D. Zino, "Simple Gaussian-beam model for GaAlAs double-heterostructure laser-diode-to-diffused-waveguide coupling calculations," Opt. Lett. **4**(9), 292–294 (1979).
19. J. C. Zhang, F. Q. Liu, S. Tan, D. Y. Yao, L. J. Wang, L. Li, J. Q. Liu, and Z. G. Wang, "High-performance uncooled distributed-feedback quantum cascade laser without lateral regrowth," Appl. Phys. Lett. **100**(11), 112105 (2012).
20. E. Kapon, J. Katz, and A. Yariv, "Supermode analysis of phase-locked arrays of semiconductor lasers," Opt. Lett. **9**(4), 125–127 (1984).
21. C. J. Corcoran and F. Durville, "Talbot cavity redesigned for increased supermode discrimination with reduced loss," Opt. Lett. **40**(13), 2957–2960 (2015).